Available online at www.sciencedirect.com
SCIENCE DIRECT
Carbohydrate Research 341 (2006) 138–152
Carbohydrate RESEARCH

Computer simulation studies of microcrystalline cellulose Iβ

James F. Matthews,[a] Cathy E. Skopec,[a] Philip E. Mason,[a] Pierfrancesco Zuccato,[a,b] Robert W. Torget,[c] Junji Sugiyama,[d] Michael E. Himmel[c,*] and John W. Brady[a,*]

[a]*Department of Food Science, Stocking Hall, Cornell University, Ithaca, NY 14853, USA*
[b]*Department of Biochemistry, Biophysics, and Macromolecular Chemistry, University of Trieste, I-34127 Trieste, Italy*
[c]*National Renewable Energy Laboratory, National Center for Bioenergy Research, 1617 Cole Boulevard, Golden, CO 80401-3393, USA*
[d]*Research Institute for Sustainable Humanosphere (RISH), Kyoto University, Uji Kyoto 611-0011, Japan*

Received 13 July 2005; accepted 27 September 2005
Available online 17 November 2005

Abstract—Molecular mechanics (MM) simulations have been used to model two small crystals of cellulose Iβ surrounded by water. These small crystals contained six different extended surfaces: (1 1 0), (1 $\bar{1}$ 0), two types of (1 0 0), and two types of (0 1 0). Significant changes took place in the crystal structures. In both crystals there was an expansion of the unit cell, and a change in the γ angle to almost orthogonal. Both microcrystals developed a right-hand twist of about 1.5° per cellobiose unit, similar to the twisting of β-sheets in proteins. In addition, in every other layer, made up of the unit cell center chains, a tilt of the sugar rings of 14.8° developed relative to the crystal plane as a result of a transition of the primary alcohol groups in these layers away from the starting TG conformation to GG. In this conformation, these groups made interlayer hydrogen bonds to the origin chains above and below. No change in the primary alcohol conformations or hydrogen-bonding patterns in the origin chain layers was observed. Strong localization of the adjacent water was found for molecules in the first hydration layer of the surfaces, due to both hydrogen bonding to the hydroxyl groups of the sugar molecules and also due to hydrophobic hydration of the extensive regions of nonpolar surface resulting from the axial aliphatic hydrogen atoms of the 'tops' of the glucose monomers. Significant structuring of the water was found to extend far out into the solution. It is hypothesized that the structured layers of water might present a barrier to the approach of cellulase enzymes toward the cellulose surfaces in enzyme-catalyzed hydrolysis, and might inhibit the escape of soluble products, contributing to the slow rates of hydrolysis observed experimentally. Since the water structuring is different for the different surfaces, this might result in slower hydrolysis rates for some surfaces compared to others.

Keywords: Cellulose Iβ; Water structuring; Molecular mechanics; Molecular dynamics; Cellulose fiber twist

1. Introduction

Cellulose, the primary structural polysaccharide of plant cell walls, is the most abundant biological molecule on earth, making up a larger fraction of the biosphere than all other biopolymers of all types combined. Like starch, which is also a polymer of D-glucose, the cellulose polysaccharide contains considerable energy stored in its C–H and C–C bonds. With the continued growth in fossil fuel consumption, the need for practical alternate fuel sources becomes ever more critical, and cellulose could potentially serve as such a renewable fuel source if an efficient method could be found to convert waste plant material into simple sugars for use in fermentation. This goal could be accomplished either by enzymatic hydrolysis of the glycosidic bonds in polysaccharides or by direct dilute acid hydrolysis.[1] The principal industrial challenge is the low hydrolysis rate using either method. The enzymatic depolymerization of insoluble cellulose, whether by exo- or endoglucanases, necessitates the removal of a cellodextran chain from the surface of the microcrystallite, as well as subsequent hydrolysis of this chain. The mechanism of enzymatic decrystallization is

* Corresponding authors. E-mail addresses: Mike_Himmel@nrel.gov; jwb7@cornell.edu

0008-6215/$ - see front matter © 2005 Elsevier Ltd. All rights reserved.
doi:10.1016/j.carres.2005.09.028

thus a key issue to be resolved before the cellulase system can be fully understood.[2] Therefore, understanding the properties of cellulose that make it so resistant to depolymerization will be of great practical use.

One of the principal limitations on cellulase activity is the insolubility of the substrate. Cellulose is the unbranched β-(1→4)-linked polymer of D-glucopyranose; the disaccharide repeat unit of this polymer is cellobiose.[3] The equatorial–equatorial β-(1→4)-linkage of cellulose produces a relatively flat ribbon-like conformation. Cellulose never occurs as a single chain, but exists from the moment of its synthesis as a crystalline array of many parallel, oriented chains, organized into microfibrils as its fundamental structural unit. The glucan chain length (degree of polymerization) varies from about 2000 to more than 15,000 glucose residues.[3,4] Cellulose can vary from the so-called elementary fibrils in plants, which contain approximately 36 cellodextrin chains, to the large microfibrils and macrofibrils of cellulosic algae, which contain more than 1200 chains.[5–7] The shape of a cellulose microfibril is determined by the geometry of the cellulose synthase complex and by the local environment.[8]

Since all of the hydroxyl groups in cellulose are equatorial, all of the axial positions are occupied by nonpolar (and non-hydrogen bonding) aliphatic protons, which means that the sides of the cellulose chain are polar and hydrogen bonding, while the tops and bottoms are hydrophobic. The chains can, therefore, stack together in a regular crystalline packing, matching up hydrophobic faces as well as allowing hydrogen bonds between chains. Microcrystalline cellulose has been shown to be made up of two different crystal phases, a triclinic form with one chain per unit cell, designated as Iα, and a lower energy, more stable monoclinic form with two nonequivalent chains per unit cell, designated as Iβ.[9,10] These crystal forms have similar molecular conformations, but alternating hydrogen-bonded sheets of Iβ are staggered by half of a glucose molecule, while the hydrogen-bonded sheets of Iα align on a constant inclined axis.[11] This relationship allows these crystal forms to be interconverted by thermal annealing.[12] While the dominant phase in higher plants is the Iβ form, and algae contain a higher proportion of Iα, both phases can be found coexisting along and across the same fibril.[13] The fibrils may consist of microcrystalline regions in which the individual cellulose chains are regularly packed in a crystalline lattice of either type, alternating with disordered regions, further along in the sequence of the same chains, where the chains are not so regularly packed. This type of structure is probably a necessary compromise between strength and rigidity and the flexibility to allow expansion, contraction, and flexing of the cell walls. Although the cellulose chain contains numerous hydrogen-bonding hydroxyl groups, this polysaccharide is completely insoluble in water under normal conditions, which of course is also necessary for it to function in its principal structural role in plant cell walls.

Cellulose occurs in the plant cell wall in a matrix of hemicelluloses and lignin, which in the biomass conversion process is disrupted prior to enzymatic treatment. The newly exposed cellulose fibrils are not well characterized in terms of the exact number of chains on each surface, but most of the fibril surface exposes the hydrophilic sides of the glucose monomers to solution. These surfaces meet at a corner where the more hydrophobic faces of the glucose monomers are exposed. Other surfaces may be exposed by mechanical rounding of corners, or by selective hydrolysis.[14] Although these surfaces are not likely to be a significant portion of the fibril surface area in plants, they may play a critical role in the activity of fungal cellulases. It has been shown that fungal-type cellulose binding modules bind specifically to the hydrophobic surfaces of large Iα crystals.[15]

In recent years the study of forces between surfaces has led to an improved understanding of the role played by hydration in keeping surfaces apart. These forces result from the structuring of layers of solvent above the surfaces, often extending far out into the bulk solvent and producing exponentially decreasing repulsive forces between the approaching surfaces.[16] The details of this solvent structuring could significantly affect the rate of diffusion of reagents toward surfaces, and thus could play an important role in determining hydrolysis rates in cellulose. Highly structured solvent at the cellulose/water interface could also substantially slow the diffusion of hydrolysis product sugars away from the surface, further slowing the rate of the hydrolysis process. The exact structure of these water layers cannot be characterized by presently available experimental techniques, but the existence of these layers can be inferred from experiments that measure the forces between two such surfaces, as has been done for lecithin bilayers[17,18] and mica.[16,19,20] However, for water structuring between cellulose surfaces, not even these types of indirect experimental probes have been reported. Attempts have been made to describe forces between cellulose surfaces by using colloidal probe and atomic force microscopy,[21,22] but these methods have not used well-defined surfaces and have not given as clear a picture as that from the lecithin and mica studies.

While the detailed structuring pattern of the water molecules making up these hydration layers cannot currently be experimentally measured, this structuring can be simulated using molecular mechanics (MM) computer calculations, as has been done for flat hydrophobic surfaces (such as the air/water interface)[23] and a hydroxylated hydrophilic surface.[24] In general, the structuring above a real surface made up of complex biological molecules with diverse functional groups might be expected to be quite complex. Recent studies

of the solvent organization around free monosaccharide molecules have revealed an intricate pattern of solvent structure extending at least to two solvation layers away from the solute.[25–27]

Heiner and Teleman have reported similar MM studies for water in contact with various cellulose surfaces, including the monoclinic (1 1 0) and (1 $\bar{1}$ 0) and triclinic (1 0 0) and (0 1 0) surfaces of cellulose crystals. They also observed significant solvent structuring, as well as structural changes, in the cellulose crystal.[28,29] Whereas torsion angles at the surface remained within 5° of the bulk crystal values, and the average pucker parameter distribution did not change at the surface, they did observe a number of transitions in the primary alcohol conformations. In these simulations the solvent density was reported where water molecules were found to prefer to occupy very specific positions, particularly between the glycosidic oxygen atom and the adjacent O-2 and O-3 hydroxyl groups. The hydration differences between the surfaces were not reported, although these workers speculated that the (1 1 0) surface is better hydrated.[28] Furthermore, the number of water molecules in the first hydration layer was similar for all surfaces and the energy of the surface cellobiose units was found to be higher than for those in the bulk crystal.[29]

The relatively recent discovery of highly crystalline and nearly pure cellulose Iα and Iβ allomorphs, along with improved methods of sample preparation, have led to significantly improved experimental analyses of cellulose structure.[11,30–34] The most recent diffraction study of cellulose Iβ structure was reported by Nishiyama et al. using synchrotron X-ray and neutron fiber diffraction.[30] These workers were able to determine the molecular structure of cellulose to better than 1 Å resolution, showing as well the hydrogen-bonding system. The results were in good agreement with the structure derived earlier by Finkenstadt and Millane.[35] Nishiyama et al. found that hydrogen bonds from HO-3 to O-5 along the same chain were consistently present, whereas the HO-6 and HO-2 hydroxyl groups formed two mutually exclusive hydrogen-bonding patterns.[30] The predominant hydrogen-bonding patterns, which accounted for approximately 75% occupancy, are shown in Figure 1. It should be noted that during the refinement, the alternate hydrogen-bond position for HO-2 in the origin chain showed zero percent occupancy and was dropped from further refinement. This resulted in an incomplete proposed alternate hydrogen-bond network. Nishiyama et al. also saw small differences in the ϕ and ψ angles between layers in the chain and in the hydroxymethyl configuration. This supports the modeling of Heiner and Teleman, who saw different hydrogen-bonding patterns for the different chains of the unit cell. Cremer–Pople pucker parameters[36] in the diffraction experiments were reported to be conformationally strained in all residues.[30]

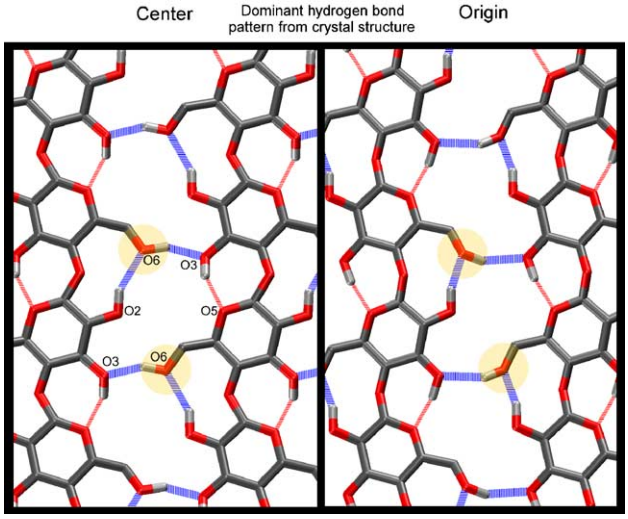

Figure 1. An illustration of the principal or predominant hydrogen-bonding patterns reported for the cellulose Iβ crystal by Nishiyama et al.[30] On the left is the center chain pattern, and on the right is the origin chain pattern. The persistent HO-3–O-5 hydrogen bonds are represented by thin dashed lines, while hydrogen bonds involving HO-6 and HO-2 are represented by thicker dashed lines. Several oxygen atoms are labeled to aid in the identification of hydrogen bonds. Two primary alcohol groups are highlighted to identify them as in the TG conformation (see Fig. 4).

In this paper we report new molecular dynamics (MD) simulations of small microcrystallites of cellulose Iβ in aqueous solution to both characterize the dynamic behavior of these crystals and the solvent structuring at the interface between the crystal surfaces and water. In these simulations, small microcrystals of finite length were immersed in water. Although periodicity was applied to the entire system 'box', the cellulose crystals themselves were not periodic and thus were free of any unnatural stresses that might arise from the application of the experimental crystallographic symmetry. One particular objective of these simulations was to determine whether the solvent structuring extends into the solution beyond the first hydration layer and whether there is any potential to affect the approach of other hydrated surfaces, as is the case for the lecithin bilayers and mica surfaces. This information might ultimately be useful in planning strategies for disrupting this solvent structuring in a way that would facilitate the diffusion of reactants and the escape of products. Another objective was to determine how the crystal structure might relax in a nonperiodic aqueous environment and whether or not the reported diffraction structure is compatible with simple models of cellulose energetics.

2. Methods

Two different microcrystallites of native cellulose Iβ were constructed using the coordinates reported by

Nishiyama et al.,[30] where the structure was inferred from X-ray fiber diffraction analysis of crystallized tunicate cellulose. This structure was reported to be a monoclinic $P2_1$ crystal with unit-cell dimension of $a = 7.784$ Å, $b = 8.201$ Å, and $c = 10.380$ Å, and $\gamma = 96.5°$. The unit cell consisted of two independent anhydroglucose units, with the chains containing them labeled as 'center' and 'origin', referring to their positions in the unit cell. Using the crystal-building facilities in CHARMM, two small crystals with different exposed crystallographic faces were fabricated. The cellooligomer chains in these crystals were all 14 monomer units in length, and hydroxyl hydrogen atoms were placed in the reported predominant hydrogen-bond pattern. Figure 2 illustrates views of both of these model crystals. One of these microcrystallites, shown on the left in the figure, contained 36 chains and emphasized the (1 1 0) and (1 $\bar{1}$ 0) surfaces. The other contained 32 chains and emphasized the (1 0 0) and (0 1 0) surfaces. Faces where center chains are on the surface are indicated by (2 0 0) or (0 2 0) to reflect their location half-way through the unit cell. (Note that the triclinic (1 0 0) and (0 1 0) surfaces studied by Heiner and Teleman differ from the monoclinic surfaces studied here.[29]) Different size crystals were chosen to keep the overall surface area as nearly equal as possible. For convenience, these two crystals will hereafter be referred to as the 'diagonal' and 'square' crystals. The square crystal has surfaces that are parallel to the unit cell axes (the 32 chain crystal shown on the right in Fig. 2), and the diagonal crystal has surfaces that cut across two unit cell axes (the 36 chain crystal on the left in Fig. 2).

All of the calculations reported here used the CHARMM molecular mechanics program.[37] The sugar atoms were modeled using parameters specifically developed for carbohydrates.[38,39] Water molecules were represented using the modified TIP3P force field.[40,41] Each of the constructed crystallites was placed in an equilibrated rectangular box of TIP3P water molecules with dimensions 56.0 Å by 56.0 Å by 89.0 Å. All those water molecules that overlapped with the carbohydrate heavy atoms were deleted. The diagonal simulation contained 6116 water molecules and 29,040 atoms in total, and the square simulation contained 6434 water molecules and 28,806 atoms.

Two-hundred steps of steepest descent minimization, followed by 100 steps of conjugate gradient minimization were first applied to the system to relieve any serious strains resulting from the setup procedure. MD simulations were then used to heat the system from 50 to 300 K in 50-K increments over a period of 10 ps, followed by an additional 190 ps of equilibration at 300 K. After this heating and equilibration stage, the system velocities were not again adjusted, and the system was simulated in the NVE ensemble using a Verlet integrator with a step size of 1 fs. Nonbonded interactions were

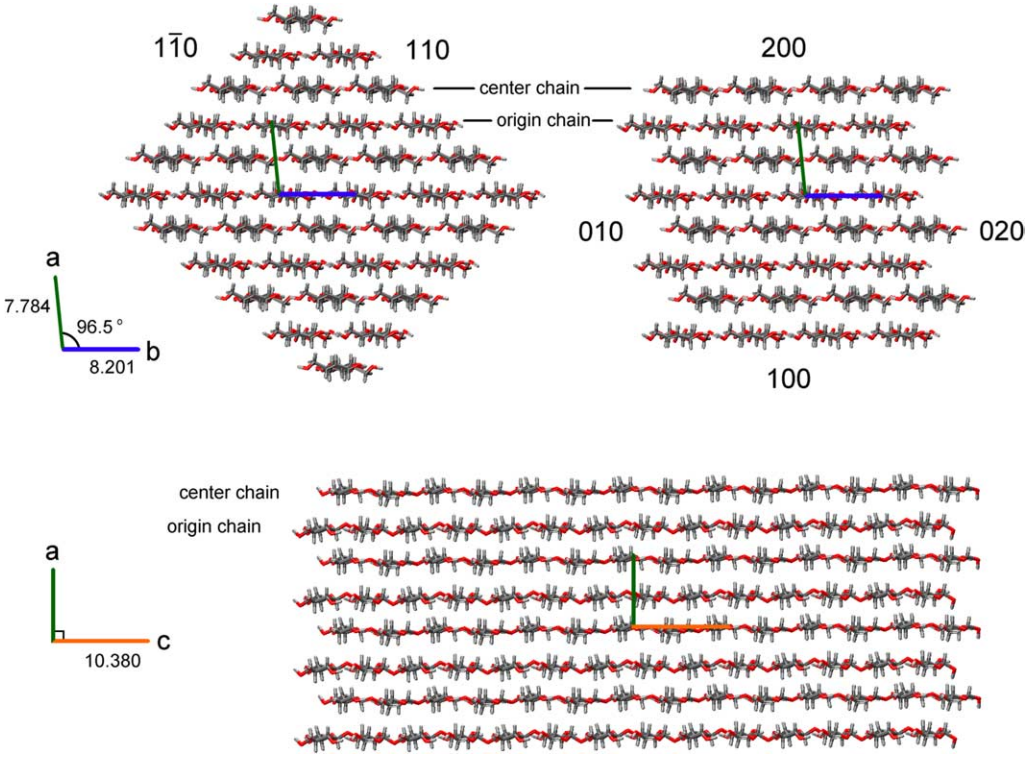

Figure 2. Views of the diagonal (left) and square (right) microcrystals as seen from their nonreducing ends, with the surfaces indicated, as well as the origin and center chain layers and unit cell axes. Opposing surfaces of the diagonal crystal have the same Miller indices. On the bottom, the square crystallite is rotated 90° to show its entire length.

truncated at 15.0 Å on a neutral group-by-neutral group basis after being made to go smoothly to zero between 12.0 and 13.0 Å using ST2-type switching functions.[37,42] Image nonbond interactions were also cut off at 15.0 Å. In all calculations, a dielectric constant of 1 was used. Chemical bond lengths involving hydrogen atoms were kept at fixed lengths using the constraint algorithm SHAKE.[43] Following equilibration, trajectories were integrated for an additional 1 ns for analysis for both systems. For comparison, an additional simulation was conducted, which was exactly like the diagonal crystal system in every respect except that dihedral angle restraining forces were used to keep the primary alcohol groups in the conformation found in the crystal. Three other simulations were carried out as a test of the sensitivity of the results to starting conditions. These test simulations consisted of (1) a simulation in which the origin chains were replaced by chains in the center chain conformation; (2) a second simulation in which the center chains were replaced by chains in the origin chain conformation; and (3) a third simulation in which the center and origin chains were interchanged.

As water molecules interact with individual functional groups in the cellulose surface, they will become localized at particular positions relative to the surface, increasing the local water density while simultaneously lowering it in immediately adjacent positions too close to be simultaneously occupied by another water molecule. Over the course of long MD simulations, the local density at each point above a surface could be calculated by dividing the region above the surface into small cubes and averaging how often water molecules occupied each cube relative to the occupancy expected in bulk liquid water. Contour maps could then be prepared showing those regions with high and low water densities. Such solvent-density mapping was applied to the present simulations using procedures developed in previous studies.[25–27,44] For the purpose of calculating solvent-density distributions, the volume of the primary system was divided into small cubes 0.30 Å in length. Complete coordinate sets were saved for every 10 fs during the simulation, and these coordinates were subsequently used to calculate the average density of water molecules in each indexed cubic box using programs developed 'in house'. The calculated densities were normalized relative to a uniform distribution in the same volume and were displayed graphically relative to the crystal surface using VMD 1.8.3.[45]

3. Results and discussion

3.1. Crystal reorganization

The starting structure for the cellulose crystal was built up from the hypothetical crystal conformation deduced from fiber-diffraction studies.[30] However, during the course of the simulations, a number of structural fluctuations and changes occurred. In the simulation of the diagonal crystal, the rms difference between the instantaneous structure and the starting crystal structure, averaged over the simulation, was 1.46 Å, while for the square-crystal simulation the rms difference was 1.72 Å. Over the length of the simulations, the average unit-cell dimensions shifted away from those reported in the diffraction study. These dimensions varied with position in the crystal, relative to the surfaces and the chain termini. Average unit cell dimensions were calculated for the central core of the crystal, ignoring surface chains and the terminal four glucose residues at each chain end. The results, averaged over these cellobiose units, are summarized in Figure 3 and compared to the crystallographic unit cell. As can be seen, in the simulation the crystal underwent an expansion which saw the value of the lattice constant a increase from 7.784 to 8.470 Å, while the b-value decreased slightly from 8.201 to 8.112 Å. The c-value expanded significantly, from 10.380 to 10.512 Å. In addition, the γ-angle decreased from 96.5° to almost orthogonal, $\gamma \approx 90°$. Reported unit-cell dimensions for cellulose Iβ vary depending on the source material[46] and expand anisotropically upon heating.[47] However, the unit cell a-axis (corresponding to the distance between hydrogen-bonded sheets) in this simulation is too different to be considered a good fit to the experimental measurements for cellulose Iβ, as is the 'monoclinic' angle near 90°. These unit-cell parameters do compare favorably with those that can be determined from the crystallographic equatorial d-spacings reported for cellulose IV_I ($a = 8.02$ Å, $b = 8.43$ Å, $\gamma = 90°$).[48] While it was previously believed that cellulose IV_I was a unique allomorph, the experimental data available at present from X-ray diffraction and NMR and FTIR spectroscopy suggest that cellulose IV_I can also be regarded as disordered cellulose Iβ.[31]

Another extremely significant change in the structure of the crystal that occurred during the simulations is that many of the C-6 primary alcohol groups underwent rotational transitions away from the conformation reported for the diffraction structure. This exocyclic group has three low-energy staggered conformations, which have been labeled TG, GG, and GT, with the first letter in these labels specifying the position of the O-6 atom as either trans or gauche with respect to the O-5 atom, and the second letter specifying its relationship to the C-4 atom (see Fig. 4).[49] In the Iβ diffraction structure, all of these exocyclic groups are in the TG conformation. In this conformation, the exocyclic hydroxyl group can make hydrogen bonds along the chain or to adjacent chains in the same layer, but no hydrogen bonds between layers (Fig. 1). For those crystal layers made up of the origin chains, there was little change in structure

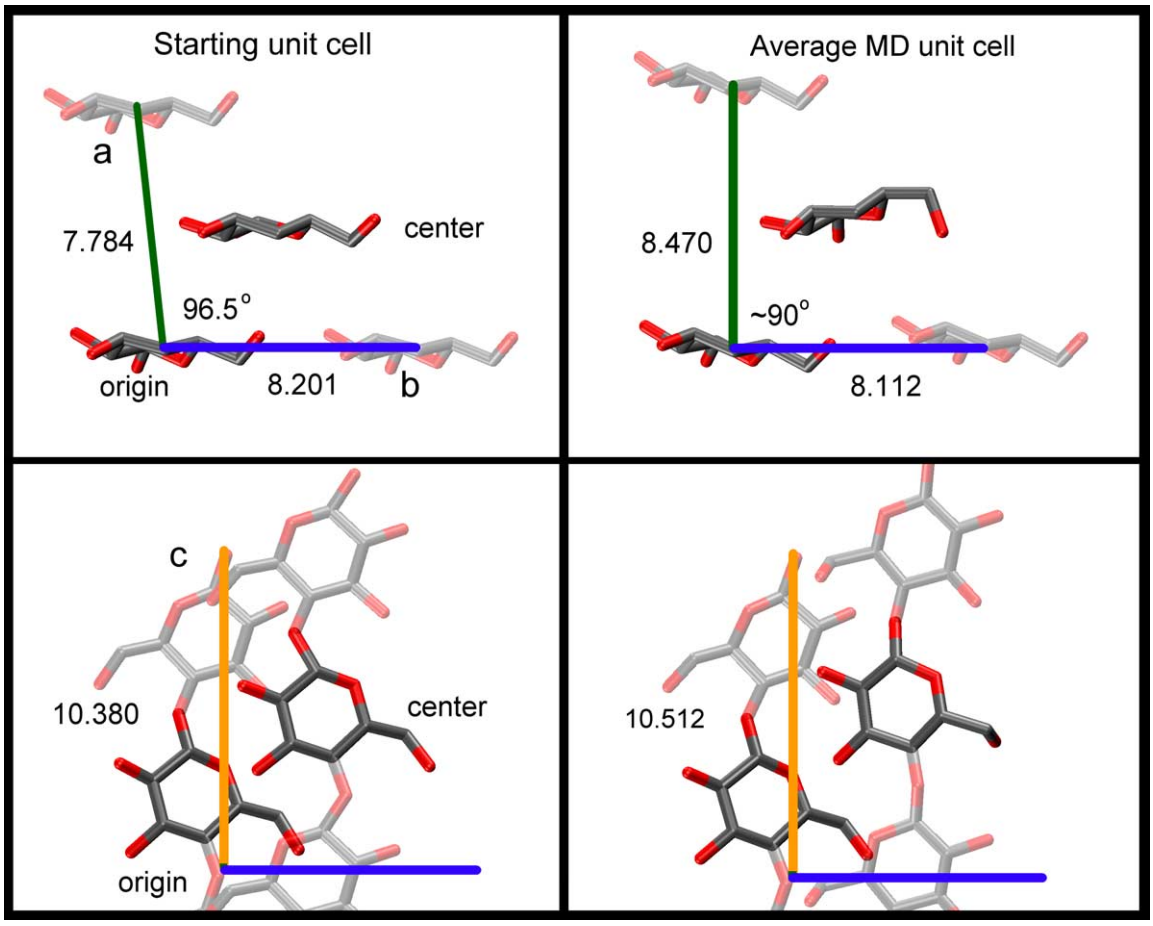

Figure 3. Left: the cellulose Iβ crystal unit cell determined by fiber diffraction; right: the trajectory-averaged unit cell for the simulation of the diagonal crystal. Hydrogen atoms are omitted for clarity, and positions obtained by symmetry operations are transparent.

in the MD simulation from that of the diffraction structure, and the hydrogen-bonding pattern remained the same (see Fig. 5). This result is remarkably similar to that of the reported experimental hydrogen-bond network in the origin chains, where the O-2 hydroxyl group was refined to just one of the two possible hydrogen-bond positions.[30]

However, in the MD simulations, in every other layer in the interior of the crystal, made up of the center chains in the diffraction structure, this primary alcohol group rotated from the starting TG conformation to the GG position. The transitions occurred randomly and were not unidirectional or permanent. Rare transitions back or to the GT conformation also occurred, but on average these transitions brought all of the residues in the center chain layers into the GG conformation. In contrast, the layers made up of origin chains remained in their original TG conformations. In this GG conformation, three rapidly interchanging hydrogen-bond patterns were possible, as shown in Figure 6. One of these patterns allowed hydrogen bonding between layers, which was not possible when the hydroxymethyl groups were in the TG conformation. On the surfaces, where the sugar monomers were in direct contact with water, the hydrogen bonds to the freely diffusing water molecules helped to introduce considerable disorder into these primary alcohol conformations and promoted frequent transitions, but the interior portions of the crystal developed a clear alternating pattern of hydroxymethyl conformations between the center and origin layers. Primary alcohol groups in surface chains alternate between facing toward the interior and facing the solvent, and the conformation of these surface groups corresponds to the local environment. Figure 4 shows a trajectory-averaged picture of hydroxymethyl conformations according to location within the microfibril. The chains are colored according to the key at the bottom of the figure, with the color determined by the predominant conformation. The top two panels show hydroxymethyl groups pointing to the right, while the bottom two panels show hydroxymethyl groups pointing to the left. Interior monomer units showed only rare transitions away from the GG conformer in center chains, and no transitions from TG in origin chains. Both inward and outward facing primary alcohol groups in surface chains showed much more diversity, sometimes exchanging between

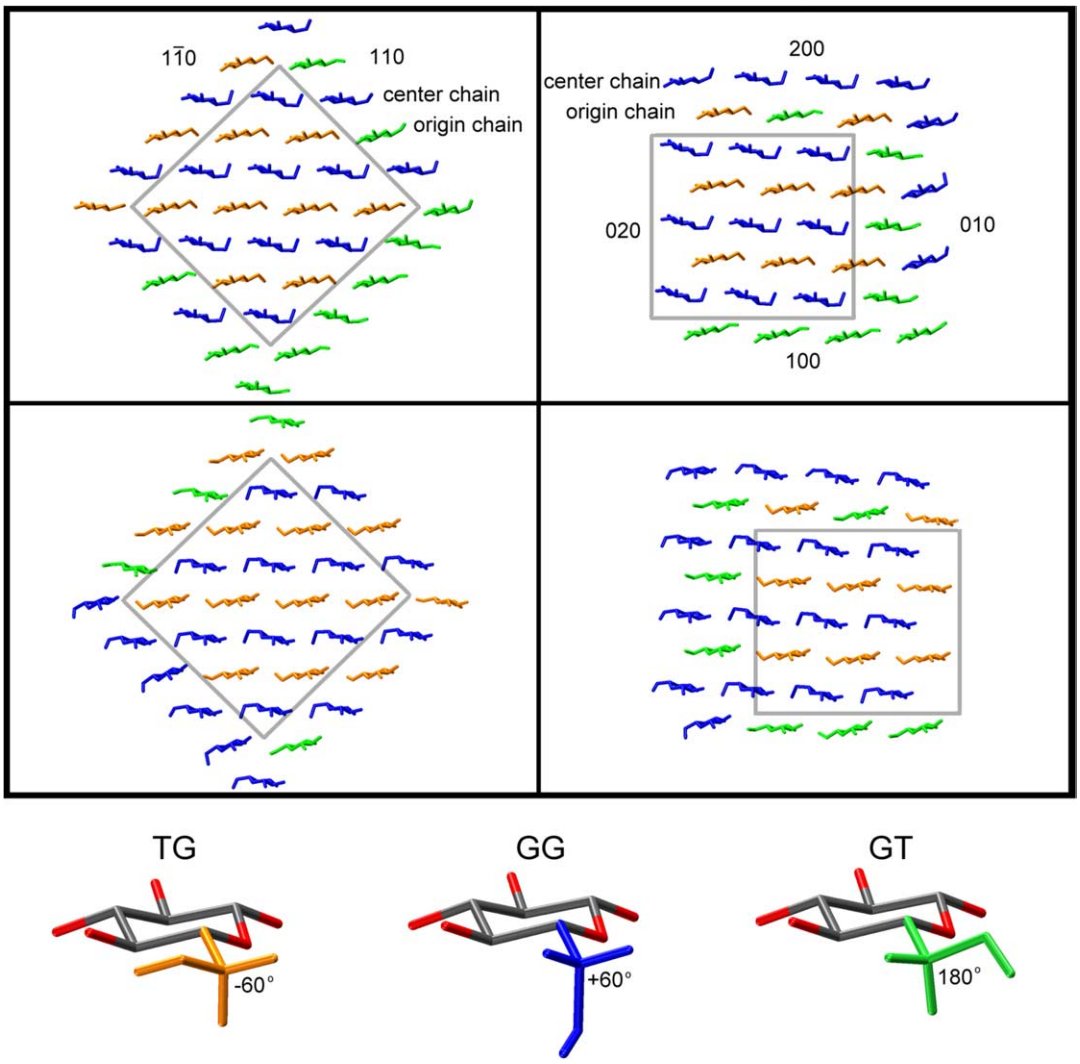

Figure 4. End views of the final structures of the two crystallites, color coded by the key at bottom to indicate the dominant primary alcohol conformations for the sugar rings in each chain. The first letter in the TG, GG, and GT labels specifies the position of the O-6 atom as either trans or gauche with respect to the O-5 atom, and the second letter specifies its relationship to the C-4 atom. The dihedral angle measured by C-4–C-5–C-6–O-6 is shown. Surface molecules generally explored two rotameric states with the color here chosen to represent the more predominant conformation. The top panels show glucosyl residues with primary alcohols pointing to the right, and the bottom panels show the next glucosyl residue along the chain that is flipped by ~180°. The regions enclosed by the grey boxes indicate that these primary alcohol conformations are nearly constant and represent the interior of the fibril.

two conformations four or five times during the 1-ns simulation. As a result there are some differences between the (1 1 0) and (1 $\bar{1}$ 0) surfaces on opposite sides of the diagonal crystal. Heiner et al. also found primary alcohol conformational changes in the layers adjacent to water.[29] Residues in their simulations were found to rotate to the GT conformation in the surface layers as was found here. Several NMR studies have determined that the conformations of surface cellulose chains are different from the interior, and as in the present simulation, contain both GG and GT rotamers.[50–52] This analysis has ignored the conformation of the four glucose units at each end of the chains, as the ends show greater disorder and swelling than does the interior. Both ends of the fibrils swelled enough to allow some water molecules to sit between layers, but waters did not penetrate significantly into the interior.

In the GG conformation, the primary alcohol groups are essentially perpendicular to the average planes of the sugar rings, and as a result are pointing up and down toward the origin chains of the layers above and below. In this conformation, the exocyclic groups can make good O-6–O-2 hydrogen bonds between layers, as is illustrated in Figure 7. Since under normal experimental conditions cellulose apparently exhibits no tendency for layers to slip relative to one another, the existence of such stabilizing hydrogen bonds may not seem so implausible. However, in this conformation, steric clashes between these center-chain primary alcohol groups and the origin layers above and below force

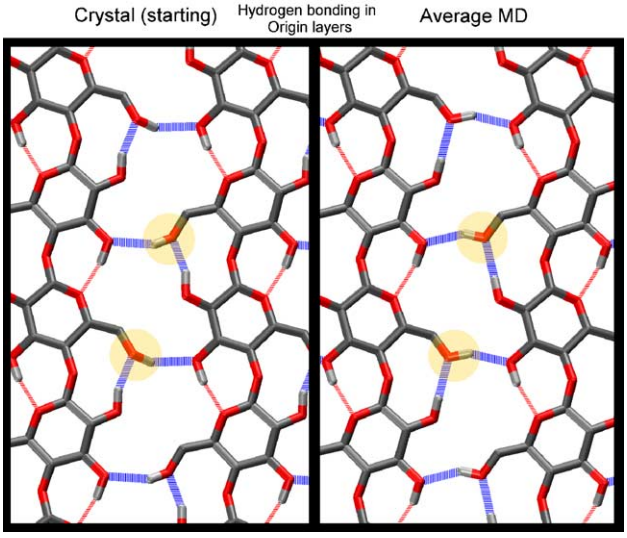

Figure 5. Left: the hydrogen-bond pattern for the origin chain layers reported from the crystal structure; right: the trajectory average hydrogen-bond pattern found for the origin chains in the MD simulation. Almost no transitions from this pattern were observed in the interior of the crystals during the 1-ns simulations. Two primary alcohols are highlighted to aid in comparison.

the center chains to tilt significantly with respect to the plane of their own layer, as is also illustrated in Figure 7. This tilt can also be clearly seen in the trajectory-averaged unit cell shown in Figure 3, and in Figure 4 as well.

Such a tilt was also found by Heiner and Teleman.[28] In their 500-ps simulations of the (1 1 0) and (1 $\bar{1}$ 0) surfaces of cellulose Iβ, the two chains in the unit cell were divided into odd and even subphases based on the angle between the glucose ring planes and the (2 0 0) plane. The angle between the layers was found to be 9.6°. The odd subphase layer was designated as the layer parallel to the (2 0 0) plane, while the even subphase was designated as that layer which tilted by 9.6°. In the present simulations, the tilting angle for the center chains was found to be 14.8°.

The transitions to the GG conformation in the present simulations are not surprising, because when using this force field,[38,39,53] the GG conformation is the lowest energy conformation for the isolated glucose residue, in good agreement with NMR experiments.[54–56] It is also lower in energy in single cellulose chains and in the glucose crystal, so that the transitions are the result of the cellulose crystal gradually annealing to its lowest energy state. Heiner and Teleman also observed GG conformations in their simulations using the GROMOS force field, approaching 35% in the so-called 'odd' chains on the (1 1 0) surface, but this conformation constituted only a minor population in the interior of the crystal and for the 'even' surface chains.[28]

As a test of the sensitivity of the observed changes in the primary alcohol conformation to the initial structure, three additional simulations of microcrystals of the same shape and dimensions as the diagonal crystal were performed. These simulations were stopped after heating and equilibration, as the structural changes occurred very rapidly. The first two were constructed either entirely of 'center' or of 'origin' chains, and the third exchanged the location of the 'center' and 'origin'

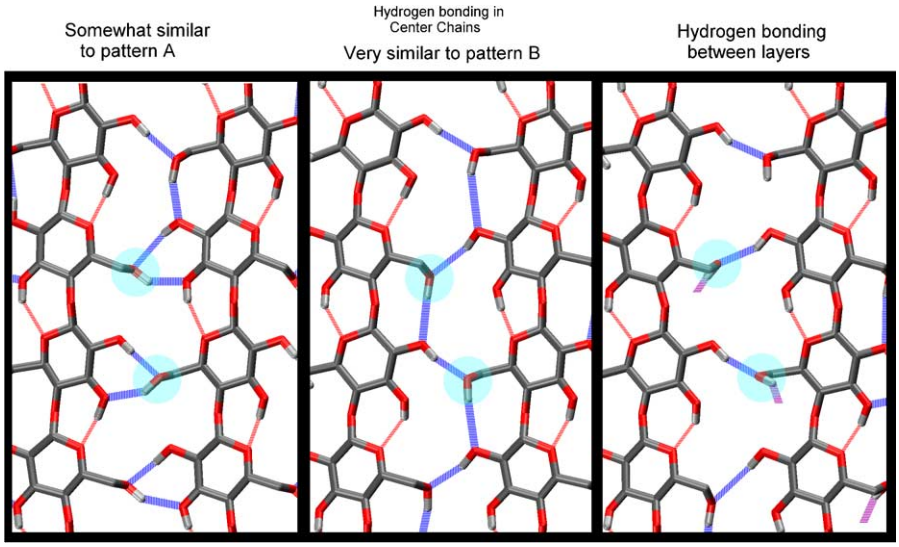

Figure 6. Single frames from the center chain layers illustrating three different hydrogen-bond patterns. Two primary alcohols are highlighted to aid in comparison. Left: similar to the predominant pattern from the crystal structure, but the rotation to GG makes the HO-2–O-6 hydrogen bond across the glycosidic linkage impossible; center: hydrogen-bond pattern is very similar to the less occupied pattern from the crystal structure; right: hydrogen bonds from HO-6 in a center chain to O-2 in an origin layer chain, which is not shown for clarity (see Fig. 7). These three patterns interchange very rapidly and are not mutually exclusive, meaning concerted motion of hydroxyl hydrogen atoms is not required to change the local hydrogen-bond pattern.

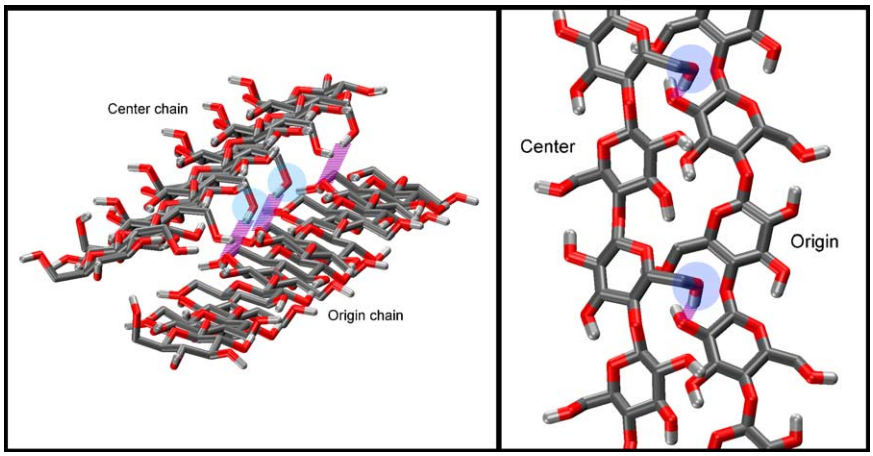

Figure 7. Views of the central portion of one center chain and one origin chain from the middle of the diagonal crystal, illustrating the interplane hydrogen bonds that can occur after the center-chain primary alcohol groups rotate to the GG conformation. Hydrogen bonds between layers are indicated with dashed lines.

chains within the unit cell. All three simulations exhibited a behavior nearly identical to that seen in the original diagonal crystal trajectory, where the primary alcohol groups of the chains located in the center of the initial unit cell rotated to the GG conformation. In addition, the individual glucose rings of these layers were forced to tilt relative to the (1 0 0) crystal layer to avoid steric clashes, as in the initial simulation. The difference in the behavior of alternating layers was not sensitive to the starting conformation, but rather to how the chains were packed relative to each other. As can be seen on the right side of Figure 7, the staggered packing of the chains allows center chains in the GG conformation to hydrogen bond to O-2 in the neighboring layer, whereas origin chains in the GG conformation would only be able to hydrogen bond to the ring oxygen O-5 in the neighboring layer (which is less polar than a hydroxyl and already hydrogen bonded to HO-3 along the same chain).

3.2. Fiber twist

Probably the most significant change that occurred in the cellulose during the simulations is that the crystal chains quickly developed a small right-hand twist during the heating and equilibration period, that then remained relatively stable throughout the rest of the simulated time. Figure 8 illustrates this twist for the diagonal crystal, with the middle hydrogen-bonded sheet shown in detail. In this figure, the average twist angle for each successive cellobiose is shown. These angles are defined as the dihedral angle for the four C-1 carbon atoms illustrated as joined by the dark lines in the figure. Although this angle varies considerably near the nonreducing end, apparently due to edge effects, in the middle of the chain the twist is fairly constant at around 1.4–1.7° per linkage, with an overall twist for this short oligosaccharide segment of almost 9.9° calculated from the first and last rows (which includes considerable irregularity due to the

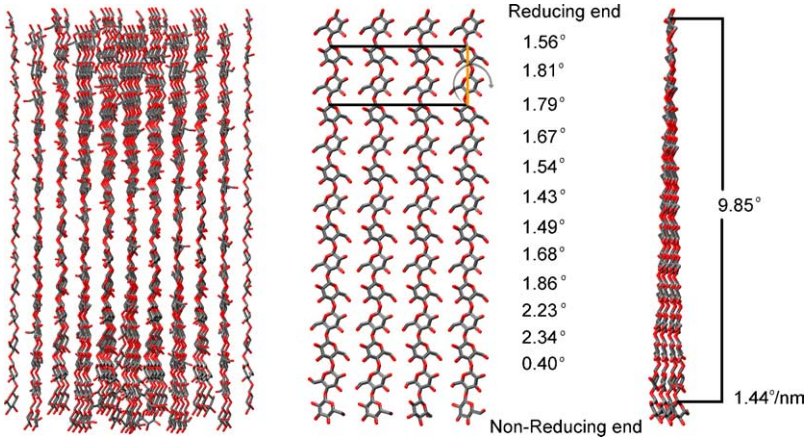

Figure 8. The trajectory average of the diagonal crystal, with a section of the central plane of the crystal seen from above and the side, illustrating the twist, which developed during the simulation. The numbers give the twist angle in degrees for each dihedral angle defined by four C-1 atoms, as at the ends of the black lines shown on the left.

highly frayed structure of the nonreducing ends). Both crystals experienced this twist, indicating that the tendency to twist is not the result of the crystallite surface geometry.

The twist in the cellulose fibers is not the result of the transitions of the primary alcohol groups in the center chains to the GG conformation. As a test of this possibility, an additional simulation was conducted for the 'diagonal' crystallite fiber in which the primary alcohol groups were constrained to remain in the TG conformation. This crystal fiber developed the same right-handed twist as was observed in the unconstrained fibril, even though all of the exocyclic groups remained TG. Thus, the twist does not depend on the primary alcohol conformation. Cellulose fibers with a right-handed twist have been observed experimentally,[57,58] and the twist of cellulose crystallites can lead to the formation of a chiral nematic phase.[59]

The enforcement of $P2_1$ symmetry confines the cellulose chains to an exact twofold helix, and this constraint can be satisfied by many combinations of torsion angles across the glycosidic linkage (reported either as $\phi_H = $ H-1–C-1–O–C-4′ and $\psi_H = $ C-1–O–C-4′–H-4′ or as $\phi_O = $ O-5–C-1–O–C-4′ and $\psi_C = $ C-1–O–C-4′–C-5′). However, the line connecting twofold helical structures for cellobiose in ϕ, ψ space does not coincide with a free-energy minimum.[53,60] Cellulose oligomers in solution are extended, but do not have a flat ribbon structure.[61,62] The preference of cellulose chains to adopt conformations away from a twofold helix is frustrated in the crystalline state by packing and hydrogen-bonding requirements. The helical angle as measured by the torsion C-5$_n$–C-2$_n$–C-2$_{n+2}$–C-5$_{n+2}$ and root mean square deviation (rmsd) of this angle for the middle six residues of each chain in the diagonal crystal are shown in Figure 9. Note that this is a different characterization than that which was used by French and Johnson[60] to avoid confusions that can arise when describing structures with near-$P2_1$ symmetry. Each of the individual interior chains departs slightly from the flat starting structure, on average forming a right-handed helix. The helix of each chain corresponds to the overall twist of the fiber in a manner similar to the twist seen in protein β-sheets.[63,64] The rmsd is greater for chains on the surface than for interior chains, reflecting increased mobility when chains are not confined in a three-dimensional lattice.

Due to the short chain length and small diameter of the model crystals, the magnitude of the twist observed in these simulations is expected to be greater than the magnitude observed for much longer or thicker microfibrils. The hydrogen-bonded sheet pattern requires that residues in neighboring chains remain in register, while the overall twist causes shear parallel to the microfibril axis. Approximating a microfibril as a cylinder of length L and radius r, over one complete revolution, the shear

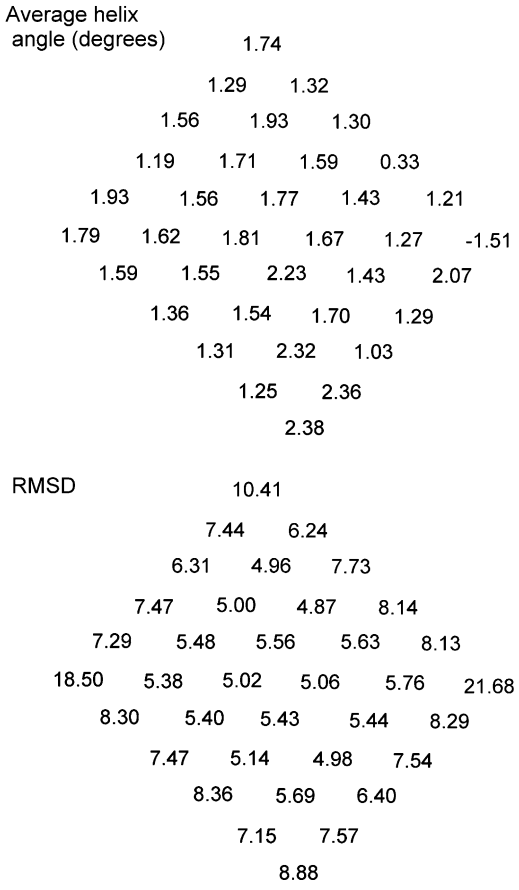

Figure 9. Average helical angle of each chain in the diagonal crystal as defined by the torsion C-5$_n$–C-2$_n$–C-2$_{n+2}$–C-5$_{n+2}$, and the rms deviation of this angle.

of surface chains relative to chains at the core is given by the relation $(4\pi^2 r^2 + L^2)^{1/2} - L$. Extending the twist observed in the diagonal simulation gives one revolution in 250 nm. With a radius of 3.60 nm, this leads to a shear of 1.02 nm per revolution, which is almost one cellobiose repeat distance. Over the length of the simulated crystals, this corresponds to a shear of approximately 1 Å, which is not unreasonable if the twist is limited by hydrogen bonding. It has been proposed that the observed differences in fiber repeat distance (c-axis) from different sources is due to interior chains that are in tension and surface chains that are in compression.[46] It is also interesting to note that bacterial cellulose ribbons have been observed to rotate during hydrolysis with certain fungal enzymes.[65]

3.3. Water structuring above the crystal surfaces

Figure 10 displays stereoviews of the contours of solvent density around both cellulose crystals, calculated from the MD simulations. This view is of a sectional slab of the crystal containing only one cellobiose unit, seen from the nonreducing end. The contour surface encloses

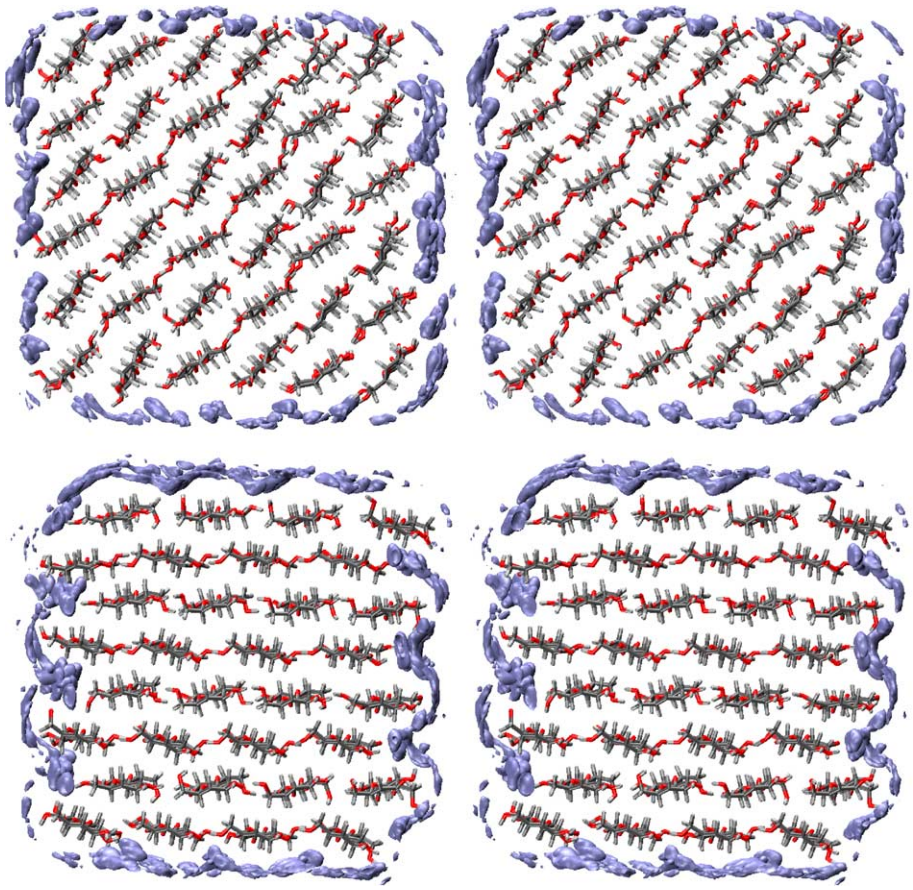

Figure 10. A stereoview of the final frames of the crystal simulations, with the trajectory-averaged solvent density contoured at a level 2.5 times bulk density. For the diagonal crystal, the top and bottom are (1 1 0) surfaces, and the left and right are (1 $\bar{1}$ 0) surfaces. For the square crystal, the surfaces are oriented as in Figure 2.

those regions in which the water density is 2.5 times that of the bulk solvent density. As can be seen from inspection of this figure, the solvent is highly structured by the cellulose surface, with water molecules occupying specific positions relative to the average positions of the sugar rings in the surface chains with very high probabilities. Furthermore, this structuring extends out into the bulk solvent water, as can be seen from Figure 11, which illustrates the solvent structuring over the (2 0 0) surface of the same crystal at a lower density contour, 1.3 times the bulk water density, as seen from the (0 0 1) face of the crystal. Water molecules above the spaces between the chains approach the crystal much more closely, as measured by their distance above the plane defined by the average positions of the glycosidic oxygen atoms. These positions consist of small ellipsoids of high densities, indicating that the water molecules that give rise to these densities are fairly constrained. These water molecules are hydrogen bonded to hydroxyl groups of the sugar residues, and the strength and geometric requirements of these hydrogen bonds strongly position the water molecules. The 'tops' of the glucose residues consist of non-hydrogen-bonding aliphatic protons, so this surface is hydrophobic. Directly above these hydrophobic surfaces of the sugar rings, the near-

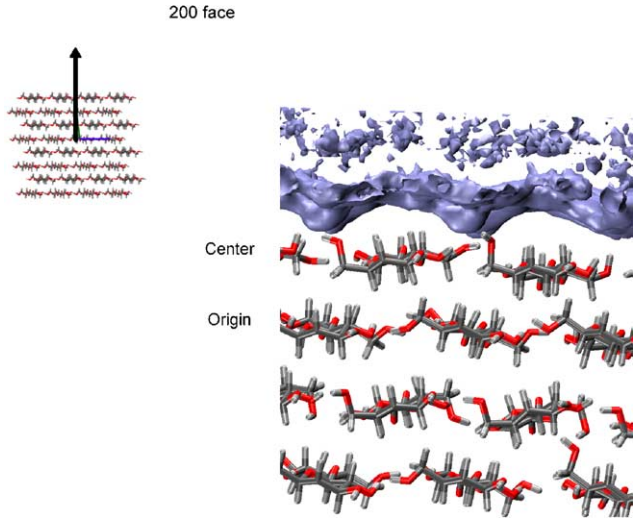

Figure 11. The water density over the (2 0 0) surface of the square crystal simulation, averaged over the trajectory. The contour encloses those regions in which the water density is greater than 1.3 times the bulk density.

est water molecules do not approach the crystal as closely, and the molecules above these positions are not as specifically localized in one particular place because they are not hydrogen bonded to the substrate. These two different types of interactions produce two discontinuous layers, or alternatively a two-tier character to the first layer, one consisting of hydrogen-bonded water molecules at a distance of approximately 2.2 Å above the glycosidic oxygen plane, and another made up of water molecules above hydrophobic surfaces centered approximately 3.6 Å above this plane. Above this upper tier is a layer in which the solvent density is below the bulk value, indicated here by an absence of density contours. A second layer of higher solvent density is found above this layer at approximately 5.5 Å. Very similar structuring is observed for the (1 0 0) surface.

Figure 12 shows the average calculated solvent density above the (0 1 0) surface, further resolved into contributions from water oxygen atoms shown in blue, and contributions from water hydrogen atoms, shown in green. As can be seen, the deeply crevassed (0 1 0) surface contains grooves deep and wide enough to accommodate water molecules, which are nonetheless so constrained by hydrogen-bonding requirements and steric clashes that they remain highly localized and oriented, such that the density contributions from the individual atoms can be resolved. Two water molecules are localized per cellobiose in these grooves, with the first receiving a hydrogen bond from the O-6 hydroxyl groups of a center chain, and donating hydrogen bonds to an O-3 hydroxyl group in a recessed origin chain and to a neighboring water. This neighboring water also receives a hydrogen bond from an O-2 in the recessed origin layer, forcing the two water hydrogen atoms to orient away from the cellulose surface.

The water structuring over the (1 1 0) and (1 $\bar{1}$ 0) surfaces is, as might be expected, intermediate between the extremes represented by these other types of surfaces. Figure 13 displays the calculated structuring for the (1 $\bar{1}$ 0) surface. As can be seen, the washboard grooves in this step face are not as deep as on the (0 1 0) surface, but nevertheless expose much more of the surface sugar residues to hydrogen-bonding interactions with the solvent, thus localizing the water molecules in relatively well-defined positions.

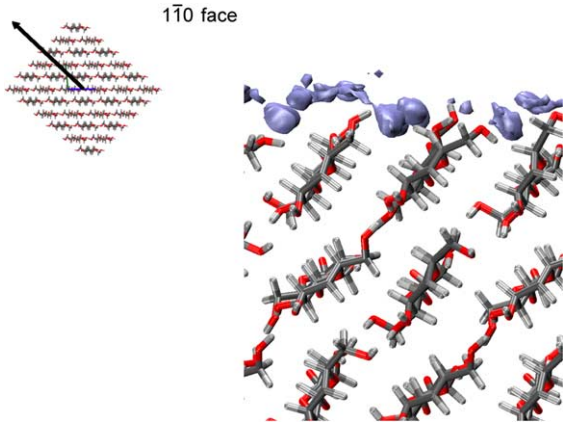

Figure 13. The water density over the (1 $\bar{1}$ 0) surface as calculated from the diagonal crystal simulation. The contour encloses those regions in which the water density is greater than 2.5 times the bulk density.

Preliminary simulations of water organization above cellulose surfaces that were constrained to remain close to the starting structure found solvent structure extending out to many layers into the liquid phase. In the present case, the microcrystallite 'protofibril' twists and flexes during the course of the simulation, which has the effect of smearing out the average positions of water molecules that are preferentially occupying positions relative to a particular feature in the surface, rather than relative to a particular point in Cartesian space. The further away from the surface, the larger the arc that will be

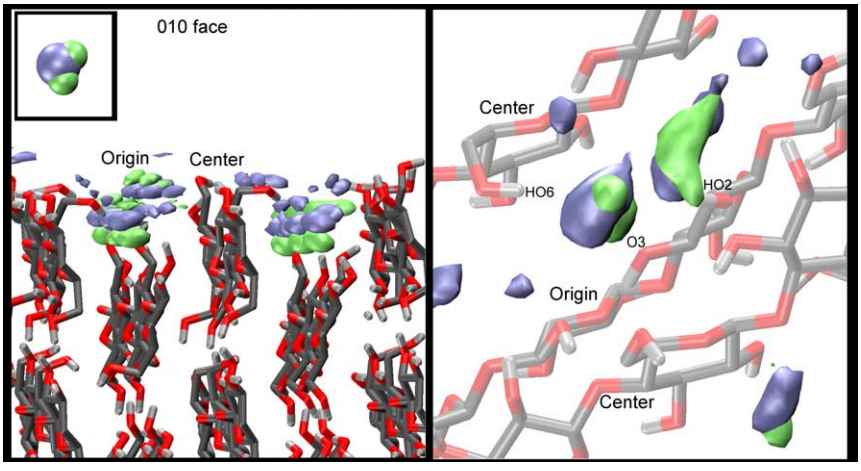

Figure 12. Side and top views of the water density over the (0 1 0) surface as calculated from the square-crystal simulation. Because of the high degree of localization of the water molecules in the surface grooves, the water oxygen density is contoured in blue, and the water hydrogen-atom density is separately contoured in green. A van der Waals representation of a water molecule with the same color convention is shown in the box at upper left.

swept out by such fluctuations, and thus the more the apparent density will be attenuated by this smearing. This does not mean, however that there is no structuring at these larger distances.

Figure 14 shows the solvent water density in one dimension, as a function of perpendicular distance from the center of the microcrystallite, averaged over the footprint of the central unit cell of each of the surfaces. These density profiles are similar for the (100) and (200) surfaces, for the (110) and $(1\bar{1}0)$ surfaces, and for the (010) and (020) surfaces, so only one of each pair is shown for clarity. As Figure 14 shows, the (200) profile exhibits three peaks (the actual maximum of the third peak lies outside the range which can be mapped with a system of this size), corresponding to three distinct hydration layers of structured water above the surface. As would be expected, the water on the (010) surface extends further into the body of the crystal due to its penetration into the deep grooves in that surface. As a result, the density profile for that surface exhibits at least five distinct peaks moving away from the surface, describing a quite complex structuring pattern. However, only one of these peaks even rises above the average bulk density, and is barely more intense than the second peak in the (200) curve. This may correspond to two types of water molecules: those confined inside the grooves, and those that are hydrogen bonded to the ridges or to the water molecules confined in the grooves. These barriers might pose an impediment to any process that requires free diffusion, such as the approach of a cellulose to the substrate or the escape of acid hydrolysis products. The differences in the structuring above the three different types of crystal faces might imply that they would be attacked and hydrolyzed at different rates by cellulase enzymes, independent of issues such as binding affinity and linkage accessibility.

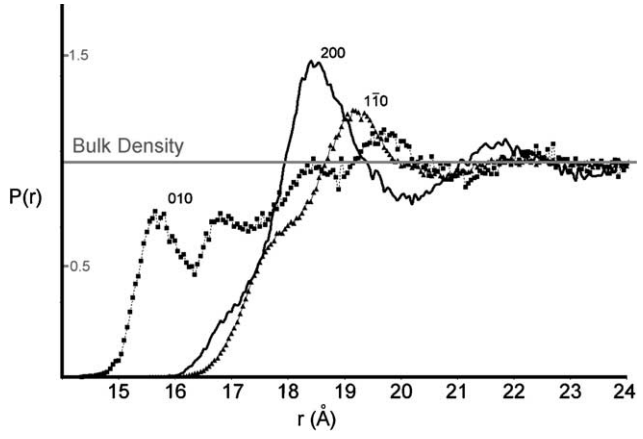

Figure 14. The solvent water density profiles as a function of distance from the center of the crystals for each type of face.

4. Conclusions

The changes observed in the crystal structures modeled in these simulations are significant. The rotation of primary alcohol groups from TG to GG in every other layer is due to the 1/4 *c*-axis shear between center and origin chains of the unit cell. The overall right-hand twist of the structures is due to the slight right-hand helix formed by each chain, similar to the twisting observed in protein β-sheets. It is always the case in simulations of this type that differences between the model and the actual behavior will arise as the result of deficiencies in the energy functions and other approximations employed in the simulations. However, it must be remembered that fiber-diffraction structures may also contain errors, as has often been the case in previous attempts to characterize the structure of cellulose. The structures found here may be a good model for cellulose IV_I, but the disordered nature of this allomorph make the experimental data difficult to interpret. In the future, comparisons between experimental diffraction patterns and virtual diffraction patterns calculated from simulations such as this should provide insight into cellulose structure. Several of the features observed here have been seen in other simulations. For example, the right-hand twist has also been observed in MD simulations of cellulose using the GLYCAM force field[66] (T. Yui et al., personal communication[67]), and may have been absent in other previous simulations simply because reported crystal periodicity was used to constrain the structures. The Yui et al. simulation also observed an expansion of the unit cell and rotations of the primary alcohol groups, including transitions to the GG conformation.[67] The previous simulations of Heiner and Teleman using the GROMOS force field also observed the tilting of the alternating center chain layers as seen here. Although errors in MD simulations are to be expected, the occurrence of these features in diverse simulations using different force fields suggest at least that the difference with the reported diffraction structure may not be the result of force-field inaccuracies, unless all of these independently developed energy functions contain the same defects. Given that the GLYCAM force field has been extensively tested against experimental data,[66] and that the CHARMM force field was also developed specifically to reproduce known monosaccharide properties,[38,39] this possibility seems unlikely.

These present simulations also demonstrate that microcrystalline cellulose surfaces highly structure the water solution in contact with them. The primary mechanism for this structuring is direct hydrogen bonding with the first layer of cellulose, which strongly localizes them in space and thus indirectly also localizes those water molecules that are hydrogen bonded with them, and so on. This highly anisotropic structuring extends at least 8 Å or more out into the solution (more than

10 Å from the van der Waals contact surface of the sugar monomers), which is at least three water layers deep. This structuring may also inhibit molecular diffusion near to the cellulose surface.

It would seem possible from the present results that water structuring by the insoluble cellulose substrate might be an important kinetic barrier to rapid hydrolysis. Previous studies of cellulolytic process have not considered the potential effect of water structuring on observed rates. For acid-catalyzed hydrolysis, the water structuring could slow the escape of cellobiose product molecules, inhibiting further hydrolysis. In the case of enzymatic hydrolysis, the diffusion of proteins toward the cellulose surface could be slowed by these water layers. If so, once adsorbed onto the surface, a processive hydrolysis mechanism (such as that of the glycosyl hydrolase family 7 cellobiohydrolases) would be faster than a mechanism, which required diffusing away and subsequently re-penetrating the hydration layers. The differences in solvent structuring between the different surfaces studied would also suggest that the (1 1 0), (1 $\bar{1}$ 0), and (0 1 0) faces of crystalline cellulose may be more susceptible to hydrolysis than the flat, hydrophobic (1 0 0) surface.

Acknowledgments

This work was supported by subcontract XCO-4-33099-01 from the National Renewable Energy Laboratory funded by the US DOE Office of the Biomass Program. The authors also thank A. D. French, R. H. Atalla, D. B. Wilson, L. Zhong, and P. Kanchanawong for helpful discussions.

References

1. Grohmann, K.; Torget, R.; Himmel, M. E. *Biotechnol. Bioeng.* **1985**, *15*, 59–80.
2. Himmel, M. E.; Ruth, M. F.; Wyman, C. E. *Curr. Opin. Biotechnol.* **1999**, *10*, 358–364.
3. Sjöström, E. *Wood Chemistry*, 2nd ed.; Academic Press: San Diego, 1993.
4. Kuga, S.; Brown, R. M. In *Biosynthesis and Biodegradation of Cellulose*; Haigler, C. H., Weiner, P. J., Eds.; Marcel Dekker: New York, 1991; pp 125–142.
5. Sugiyama, J.; Harada, H.; Fujiyoshi, Y.; Uyeda, N. *Planta* **1985**, *166*, 161–168.
6. Newman, R. H. *Solid State Nucl. Magn. Reson.* **1999**, *15*, 21–29.
7. Koyama, M.; Sugiyama, J.; Itoh, T. *Cellulose* **1997**, *4*, 147–160.
8. Doblin, M. S.; Kurek, I.; Jacob-Wilk, D.; Delmer, D. P. *Plant Cell. Physiol.* **2002**, *43*, 1407–1420.
9. Sugiyama, J.; Vuong, R.; Chanzy, H. *Macromolecules* **1991**, *24*, 4168–4175.
10. Atalla, R. H.; VanderHart, D. L. *Science* **1984**, *223*, 283–285.
11. Nishiyama, Y.; Sugiyama, J.; Chanzy, H.; Langan, P. *J. Am. Chem. Soc.* **2003**, *125*, 14300–14306.
12. Yamamoto, H.; Horii, F.; Odani, H. *Macromolecules* **1989**, *22*, 4132–4134.
13. Imai, T.; Sugiyama, J. *Macromolecules* **1998**, *31*, 6275–6279.
14. Helbert, W.; Nishiyama, Y.; Okano, T.; Sugiyama, J. *J. Struct. Biol.* **1998**, *124*, 42–50.
15. Lehtiö, J.; Sugiyama, J.; Gustavsson, M.; Fransson, L.; Linder, M.; Teeri, T. T. *Proc. Natl. Acad. Sci. U.S.A.* **2003**, *100*, 484–489.
16. Israelachvili, J. *Intermolecular and Surface Forces*, 2nd ed.; Academic Press: London, 1992.
17. LeNeveu, D. M.; Rand, R. P.; Parsegian, V. A. *Nature* **1976**, *259*, 601–603.
18. LeNeveu, D. M.; Rand, R. P.; Parsegian, V. A.; Gingell, D. *Biophys. J.* **1977**, *18*, 209–230.
19. Israelachvili, J. N.; Pashley, R. M. *Nature* **1983**, *306*, 249–250.
20. Israelachvili, J.; Pashley, R. *Nature* **1982**, *300*, 341–342.
21. Leporatti, S.; Sczech, R.; Riegler, H.; Bruzzano, S.; Storsberg, J.; Loth, F.; Jaeger, W.; Laschewsky, A.; Eichhorn, S.; Donath, E. *J. Colloid Interface Sci.* **2005**, *281*, 101–111.
22. Notley, S. M.; Pettersson, B.; Wågberg, L. *J. Am. Chem. Soc.* **2004**, *126*, 13930–13931.
23. Lee, C. Y.; McCammon, J. A.; Rossky, P. J. *J. Chem. Phys.* **1984**, *80*, 4448–4455.
24. Lee, S. H.; Rossky, P. J. *J. Chem. Phys.* **1994**, *100*, 3334–3345.
25. Schmidt, R. K.; Karplus, M.; Brady, J. W. *J. Am. Chem. Soc.* **1996**, *118*, 541–546.
26. Liu, Q.; Brady, J. W. *J. Am. Chem. Soc.* **1996**, *118*, 12276–12286.
27. Liu, Q.; Schmidt, R. K.; Teo, B.; Karplus, P. A.; Brady, J. W. *J. Am. Chem. Soc.* **1997**, *119*, 7851–7862.
28. Heiner, A. P.; Teleman, O. *Langmuir* **1997**, *13*, 511–518.
29. Heiner, A. P.; Kuutti, L.; Teleman, O. *Carbohydr. Res.* **1998**, *306*, 205–220.
30. Nishiyama, Y.; Langan, P.; Chanzy, H. *J. Am. Chem. Soc.* **2002**, *124*, 9074–9082.
31. Wada, M.; Heux, L.; Sugiyama, J. *Biomacromolecules* **2004**, *5*, 1385–1391.
32. Wada, M.; Chanzy, H.; Nishiyama, Y.; Langan, P. *Macromolecules* **2004**, *37*, 8548–8555.
33. Kono, H.; Erata, T.; Takai, M. *J. Am. Chem. Soc.* **2002**, *124*, 7506–7511.
34. Kono, H.; Erata, T.; Takai, M. *Macromolecules* **2003**, *36*, 3589–3592.
35. Finekenstadt, V. L.; Millane, R. P. *Macromolecules* **1998**, *31*, 7776–7783.
36. Cremer, D.; Pople, J. A. *J. Am. Chem. Soc.* **1975**, *97*, 1354–1358.
37. Brooks, B. R.; Bruccoleri, R. E.; Olafson, B. D.; Swaminathan, S.; Karplus, M. *J. Comput. Chem.* **1983**, *4*, 187–217.
38. Palma, R.; Zuccato, P.; Himmel, M. E.; Liang, G.; Brady, J. W. In *Glycosyl Hydrolases in Biomass Conversion*; Himmel, M. E., Ed.; American Chemical Society: Washington, DC, 2000; pp 112–130.
39. Kuttel, M.; Brady, J. W.; Naidoo, K. J. *J. Comput. Chem.* **2002**, *23*, 1236–1243.
40. Jorgensen, W. L.; Chandrasekhar, J.; Madura, J. D.; Impey, R. W.; Klein, M. L. *J. Chem. Phys.* **1983**, *79*, 926–935.
41. Durell, S. R.; Brooks, B. R.; Ben-Naim, A. *J. Phys. Chem.* **1994**, *98*, 2198–2202.

42. Stillinger, F. H.; Rahman, A. *J. Chem. Phys.* **1974**, *60*, 1545–1557.
43. van Gunsteren, W. F.; Berendsen, H. J. C. *Mol. Phys.* **1977**, *34*, 1311–1327.
44. Brady, J. W. *Forefronts/Cornell Theory Center* **1993**, *9*, 7.
45. Humphrey, W.; Dalke, A.; Schulten, K. *J. Mol. Graphics* **1996**, *14*, 33–38.
46. Davidson, T. C.; Newman, R. H.; Ryan, M. J. *Carbohydr. Res.* **2004**, *339*, 2889–2893.
47. Wada, M. *J. Polym. Sci., Part B: Polym. Phys.* **2002**, *40*, 1095–1102.
48. Aravindanath, S.; Sreenivasan, S.; Iyer, P. B. *J. Polym. Sci., Part C: Polym. Lett.* **1986**, *24*, 207–209.
49. Marchessault, R. H.; Peréz, S. *Biopolymers* **1979**, *18*, 2369–2374.
50. Viëtor, R. J.; Newman, R. H.; Ha, M.-A.; Apperley, D. C.; Jarvis, M. C. *The Plant J.* **2002**, *30*, 721–731.
51. Newman, R. H.; Davidson, T. C. *Cellulose* **2004**, *11*, 23–32.
52. Sturcová, A.; His, I.; Apperley, D. C.; Sugiyama, J.; Jarvis, M. C. *Biomacromolecules* **2004**, *5*, 1333–1339.
53. Kuttel, M. M. Ph.D. thesis, University of Cape Town: Cape Town, 2003, p. 141.
54. Bock, K.; Duus, J. Ø. *J. Carbohydr. Chem.* **1994**, *13*, 513–543.
55. Nishida, Y.; Ohrui, H.; Meguro, H. *Tetrahedron Lett.* **1984**, *25*, 1575–1578.
56. Horii, F.; Hirai, A.; Kitamaru, R. In *The Structures of Cellulose: Characterization of the Solid States*; Atalla, R. H., Ed.; American Chemical Society: Washington, DC, 1987; pp 119–134.
57. Hanley, S. J.; Revol, J.-F.; Godbout, L.; Gray, D. G. *Cellulose* **1997**, *4*, 209–220.
58. Hirai, A.; Tsuji, M.; Horii, F. *Senri Gakkai shi* **1998**, *54*, 506–510.
59. Fleming, K.; Gray, D. G.; Matthews, S. *Chem. Eur. J.* **2001**, *7*, 1831–1835.
60. French, A. D.; Johnson, G. P. *Cellulose* **2004**, *11*, 5–22.
61. Almond, A.; Sheehan, J. K. *Glycobiology* **2003**, *13*, 255–264.
62. Sugiyama, H.; Hisamichi, K.; Usui, T.; Sakai, K.; Ishiyama, J.-I. *J. Mol. Struct.* **2000**, *556*, 173–177.
63. Chothia, C. *J. Mol. Biol.* **1973**, *7*, 295–302.
64. Ho, B. K.; Curmi, P. M. G. *J. Mol. Biol.* **2002**, *317*, 291–308.
65. Bowling, A. J.; Amano, Y.; Lindstrom, R.; Brown, R. M. *Cellulose* **2001**, *8*, 91–97.
66. Woods, R. J.; Dwek, R. A.; Edge, C. J.; Fraser-Reid, B. *J. Phys. Chem.* **1995**, *99*, 3832–3846.
67. Yui, T.; Akiba, S.; Hayashi, S. *Carbohydr. Res.*, submitted for publication.